

Hexagonal Lyotropic Liquid Crystal from Simple “Abiotic” Foldamers

Yu Chen,^[a, b] Zhiqiang Zhao,^[a, b] Zheng Bian,^{*[a]} Rizhe Jin,^[a] Chuanqing Kang,^[a] Xuepeng Qiu,^[a] Haiquan Guo,^[a] Zhijun Du,^[a] and Lianxun Gao^[a]

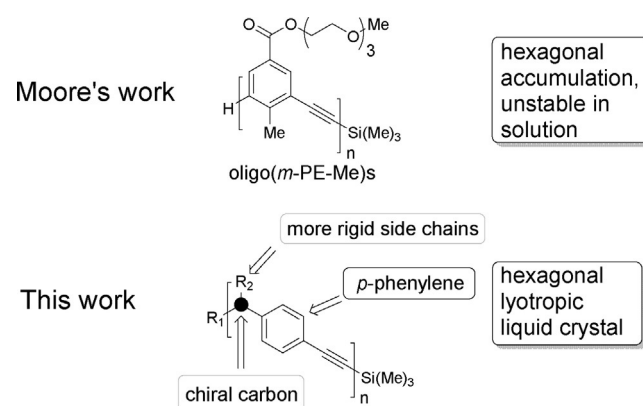
The motivation of foldamer chemistry is to identify novel building blocks that have the potential to imitate natural species. Peptides and peptide mimetics can form stable helical conformations and further self-assemble into diverse aggregates in water, where it is difficult to isolate a single helix. In contrast, most “abiotic” foldamers may fold into helical structures in solution, but are difficult to assemble into tertiary ones. It remains a challenge to obtain “abiotic” species similar to peptides. In this paper, a novel foldamer scaffold, in which *p*-phenyleneethynylene units are linked by chiral carbon atoms, was

designed and prepared. In very dilute solutions, these oligomers were random coils. The hexamer and octamers could form a hexagonal lyotropic liquid crystal (LC) in CH₂Cl₂ when the concentrations reached the critical values. The microscopic observations indicated that they could assemble into the nanofibers in the LC. Interestingly, after some LC phases were diluted at room temperature, the nanofibers could be preserved. The good stabilities of the assemblies are possibly attributed to a more compact backbone and more rigid side chains.

1. Introduction

Foldamers are created to imitate natural species such as proteins and DNA.^[1–6] It is the most important goal for foldamer chemists to thoroughly understand complex assembly behaviours of natural species and to perform similar biological functions. As natural counterparts, many artificial peptides could form stable helical conformations and further self-assemble into diverse aggregates. In contrast, “abiotic” foldamers, such as oligo(*m*-phenyleneethynylene)s [oligo(*m*-PE)s] and aromatic tertiary amides, for example, seemed to be too “cosy” to further aggregate towards tertiary or quaternary folds, whereas the second structure of them all, no matter if it was a helix or a coil, could be well adjusted in solution.^[4–6,8] In particular, “abiotic” foldamer-based liquid crystals (LCs) are seldom reported, although they are popular for peptidomimetics.^[7,9]

Notably, Moore and co-workers have found that oligo(*m*-PE-Me)s could form a hexagonal structure with helical backbones in the solid state (Scheme 1).^[10] Yashima and co-workers have



Scheme 1. A comparison of Moore's work and this work.

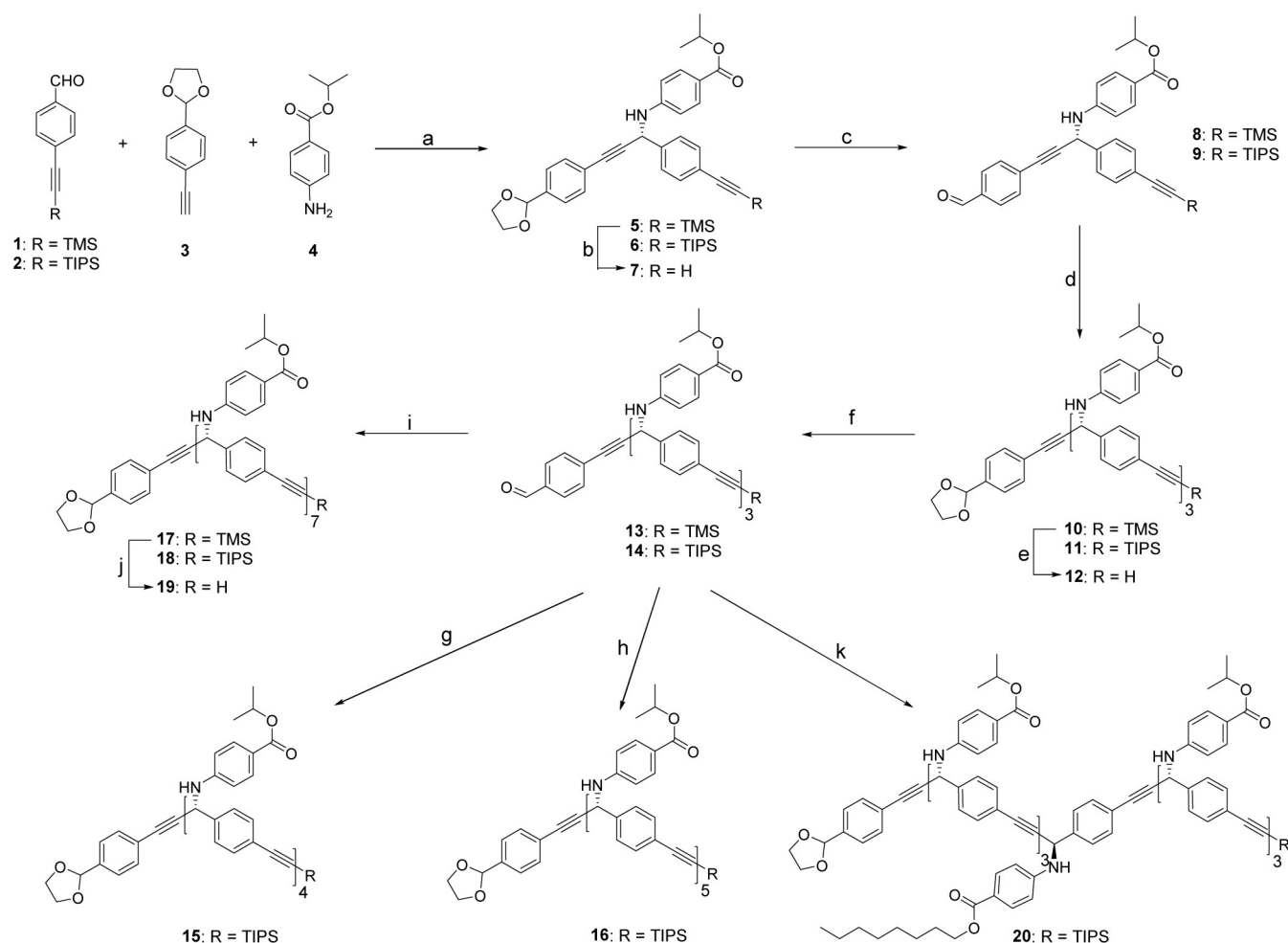
reported that poly(*m*-PE)s with amide side chains also form a similar structure.^[11] A hexagonal PE-based LC phase has not yet been reported, although hexagonal LCs are common. Onsager's theory predicts that assemblies of molecules with a high aspect ratio will spontaneously form a LC phase above a critical concentration through an entropy-driven process.^[12] However, it seemed difficult for a large number of *m*-PE-based foldamers reported previously to assemble into such fibres.^[4] We plan to rebuild the classic PE scaffold, so as to realise a higher-order fold in the fluid. Our new strategy is that linear *p*-PEs are simply linked by chiral carbon atoms (Scheme 1). The introduc-

[a] Y. Chen, Z. Zhao, Dr. Z. Bian, Dr. R. Jin, Dr. C. Kang, Dr. X. Qiu, Dr. H. Guo, Dr. Z. Du, Dr. L. Gao
State Key Laboratory of Polymer Physics and Chemistry
Changchun Institute of Applied Chemistry
Chinese Academy of Sciences
Changchun 130022 (P. R. China)
E-mail: bianzh@ciac.ac.cn
chenyu@ciac.ac.cn

[b] Y. Chen, Z. Zhao
University of Chinese Academy of Sciences
Beijing 100049 (P. R. China)

Supporting Information for this article can be found under <http://dx.doi.org/10.1002/open.201600007>.

© 2016 The Authors. Published by Wiley-VCH Verlag GmbH & Co. KGaA. This is an open access article under the terms of the Creative Commons Attribution-NonCommercial-NoDerivs License, which permits use and distribution in any medium, provided the original work is properly cited, the use is non-commercial and no modifications or adaptations are made.



Scheme 2. The synthetic routes of chiral foldamers. Reaction conditions: a) $\text{CuBF}_4(\text{CH}_3\text{CN})_4$, tri(*o*-tolyl)phosphine, *N*-Boc-*L*-proline, MS 3 Å, 3–5 °C, 7 d, CH_2Cl_2 , 70% for **5**, 73% for **6**; b) CsF, AcOH, 60 °C, 5 h, THF, 95%; c) $\text{BF}_3\text{-Et}_2\text{O}$, 60 °C, 5 h, THF/ H_2O , > 98%; d) **7**, **4**, $\text{CuBF}_4(\text{CH}_3\text{CN})_4$, tri(*o*-tolyl)phosphine, *N*-Boc-*L*-proline, MS 3 Å, 3–5 °C, 7 d, CH_2Cl_2 , 61% for **10**, 65% for **11**; e) CsF, AcOH, 60 °C, 6 h, THF, 91%; f) $\text{BF}_3\text{-Et}_2\text{O}$, 60 °C, 6 h, THF/ H_2O , > 95%; g) **3**, **4**, $\text{CuBF}_4(\text{CH}_3\text{CN})_4$, tri(*o*-tolyl)phosphine, *N*-Boc-*L*-proline, MS 3 Å, 20 °C, 1 d, CH_2Cl_2 , 26%; h) **7**, **4**, $\text{CuBF}_4(\text{CH}_3\text{CN})_4$, tri(*o*-tolyl)phosphine, *N*-Boc-*L*-proline, MS 3 Å, 30 °C, 3 d, CH_2Cl_2 , 31%; i) **12**, **4**, $\text{CuBF}_4(\text{CH}_3\text{CN})_4$, tri(*o*-tolyl)phosphine, *N*-Boc-*L*-proline, MS 3 Å, 30 °C, 5 d, CH_2Cl_2 , 30% for **17**, 35% for **18**; j) CsF, AcOH, 60 °C, 5 h, THF, 85%; k) **12**, *n*-octyl 4-aminobenzoate, $\text{CuBF}_4(\text{CH}_3\text{CN})_4$, tri(*o*-tolyl)phosphine, *N*-Boc-*L*-proline, MS 3 Å, 30 °C, 3 d, CH_2Cl_2 , 26%. TMS, trimethylsilyl; TIPS, triisopropylsilyl; Boc, *tert*-butyloxycarbonyl.

tion of chiral elements could favour the formation of helical scaffolds and further assembly.^[13–14] In this paper, a series of chiral methylene-*p*-phenyleneethynylene (Mp-PE) oligomers with 4-isopropoxycarbonyl phenylamino side groups were successfully prepared (Scheme 2). The hexamers and octamers can form the hexagonal lyotropic LC phases in CH_2Cl_2 as the concentrations reach the critical values. Here, we present the results and corresponding analyses.

2. Results and Discussion

Notably, Moore and co-workers have designed many foldamers with a twist-sense bias by introducing a single chiral unit to the *m*-PE backbone.^[13a,e] In contrast, the Mp-PE scaffold is closer to a peptide structure with rigid amide units linked by chiral carbon atoms. To construct the chiral carbon in Mp-PE oligomers, the slightly modified asymmetric Mannich addition of alkyne to imine with $\text{CuBF}_4(\text{CH}_3\text{CN})_4$ and *N*-Boc-*L*-proline as

catalysts was utilised (Scheme 2).^[15] The enantiomeric excesses of (*R*)-dimers **5** and **6** may reach > 99% from 92–95% after one recrystallisation procedure (Figures S1 and S2). The single crystal of (*R*)-dimer **5** was obtained by slow evaporation of CH_2Cl_2 /*n*-hexane solution (Figure 1). (*R,R,R*)-Tetramers **10** and **11** were prepared from enantiopure de-protected dimer aldehyde and alkyne. In product **11**, the (*R,S,R*)-diastereomer was hardly detected by using HPLC (Figure 2a). Moreover, (*R,R,R,R*)-pentamer **15** was prepared from **11**, and its (*R,R,R,S*)-diastereomer was also hardly detected (Figure 2b). The asymmetric reaction based on enantiopure substrates gave the enantiopure all-*R* products, whether the newly formed chiral carbon was located on the end or centre of the main chain. (*R,R,R,R,R*)-Hexamer **16** and (*R,R,R,R,R,R*)-octamers **17**, **18**, and **20** were prepared by using a similar procedure.^[16] Compound **19** was the de-TMS product of **17**. The structures of the oligomers were confirmed by using NMR, IR and high-resolution MS techniques. Compound **17** was contaminated with a small amount of **19**. Un-

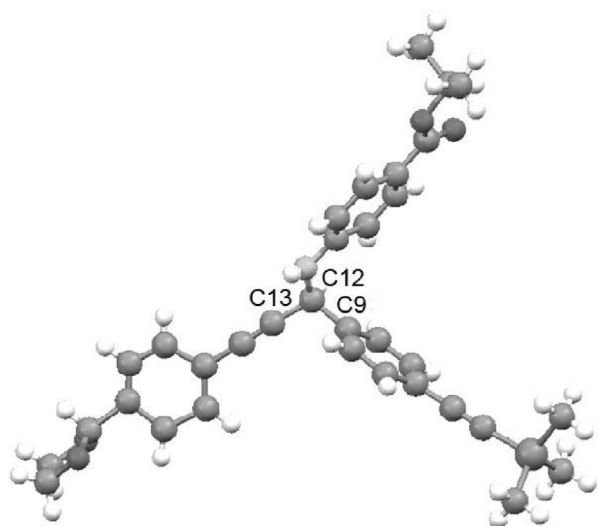


Figure 1. The single-crystal structure of (*R*)-dimer **5**. The angle C13–C12–C9: 110.35°. Crystal data for **1**: C₃₃H₃₅NO₄Si; Mr = 537.71; Triclinic; space group, *P*1; *a* = 8.4991(9) Å, *b* = 9.6789(10) Å, *c* = 10.3917(10) Å; α = 84.461(2)°, β = 82.866(2)°, γ = 69.252(2)°.^[23]

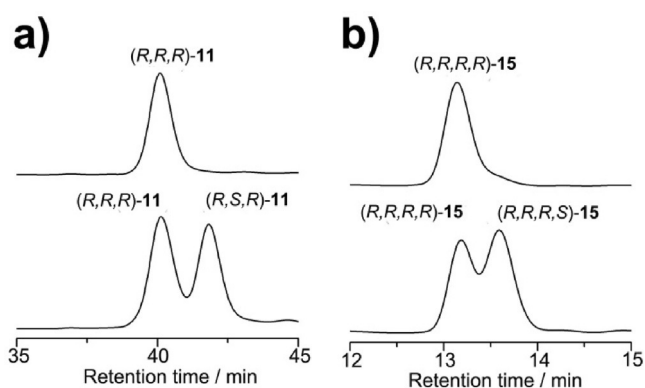


Figure 2. HPLC analysis of a) (*R,R,R*)-**11** and b) (*R,R,R,R*)-**15** using CHIRALPAK ID. Eluent: *n*-hexane/*iso*-propanol/CH₂Cl₂ (v:v:v) = 17.5:65:17.5 for (*R,R,R*)-**11**, 0.2 mL min⁻¹; *iso*-propanol/CH₂Cl₂ (v:v) = 60:40 for (*R,R,R,R*)-**15**, 0.2 mL min⁻¹. The (*R,S,R*) and (*R,R,R,S*) diastereomers were prepared with *N*-Boc-*D*-proline as the catalyst.

fortunately, it was difficult to synthesise a longer oligomer, owing to the poor solubility of reaction substrates with five or more repeating units.

In the initial solubility test, we found that 3 wt% **18** in CH₂Cl₂ at room temperature formed a translucent fluid, which is characteristic of an LC phase. Then, we used optical microscopy to evaluate whether all of the oligomer solutions form an LC phase or not. All of the samples in different solvents were prepared by heating the oligomers in a sealed tube at 90 °C for 10 min, and then keeping them at room temperature for 2 h with slow stirring. The oligomer samples were drawn into microcapillaries and examined between cross-polarising filters at room temperature (Figure 3). In general, the observation of birefringence is taken as evidence of LC phase formation.^[17] No birefringence was observed for concentrations of up to 5 wt% **10** or **11** and up to 3 wt% **15**, whereas only 2 wt% **16**, **18**, and

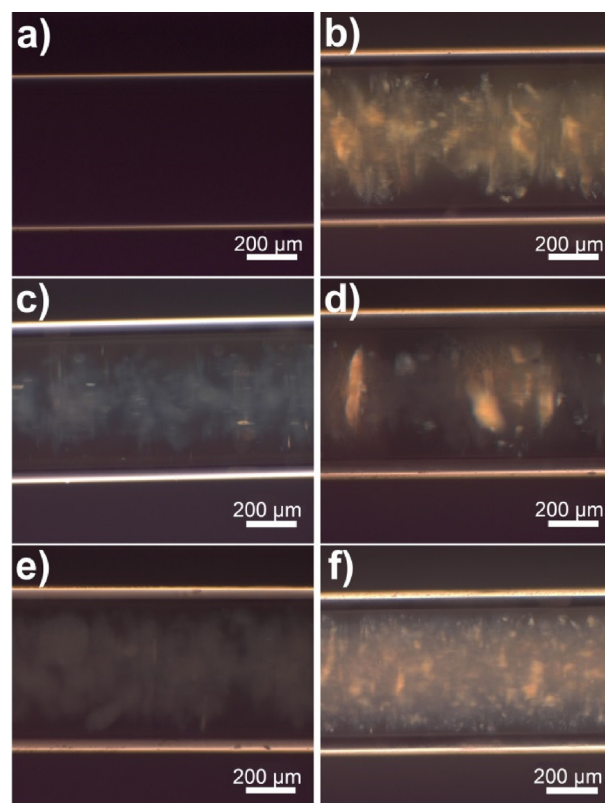


Figure 3. Polarising optical microscope images of a) **11**, 5 wt%; b) **16**, 2 wt%; c) **17**, 1 wt%; d) **18**, 2 wt%; e) **19**, 1 wt%; f) **20**, 2 wt% in CH₂Cl₂. The birefringence phenomena were observed at critical concentrations.

20, as well as 1 wt% **17** and **19** in CH₂Cl₂ displayed birefringence. Different groups on the terminal alkyne [Si(*i*Pr)₃, SiMe₃ and H] and the substitution of one *n*-C₈H₁₇ group in the side chains did not affect LC phase formation. The smoky optical textures suggested the existence of a hexagonal LC phase.^[18] In contrast, **16–20** in CHCl₃, THF, DMF or DMSO did not form an LC phase. Notably, the diastereomers with one (*S*)-carbon, such as (*R,R,R,S,R,R,R*)-**18**, also displayed good solubility and no birefringence. Interestingly, 5 wt% **15** in CH₂Cl₂ can form a gel at room temperature (Figure S3).

The ²H NMR measurements can be used to characterise the LC phase. If an LC phase is formed in CD₂Cl₂, the quadrupolar coupling between the D atoms gives rise to characteristic ²H NMR line shapes.^[19] Figure 4b showed that the ²H NMR

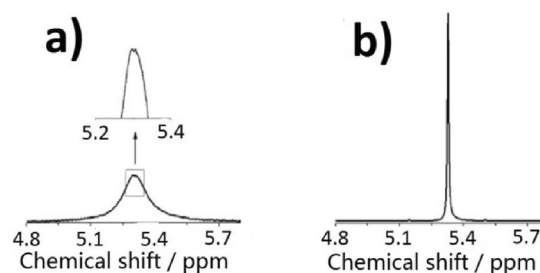


Figure 4. ²H NMR spectra of a) 3 wt% and b) 0.1 wt% **18** in CD₂Cl₂ at room temperature.

spectra of 0.1 wt% **18** in CD_2Cl_2 gave a sharp single peak for the CD_2Cl_2 resonance. In contrast, the ^2H NMR signal of 3 wt% **18** in CD_2Cl_2 was evidently broadened and a slight split was observed (Figure 4a), indicating the existence of an LC phase.

We also performed powder X-ray diffraction (PXRD) experiments to characterise the microstructure of the assemblies. The solids of **16–20**, prepared by slow evaporation of LC phases, gave similar PXRD patterns (Figure 5), suggesting the

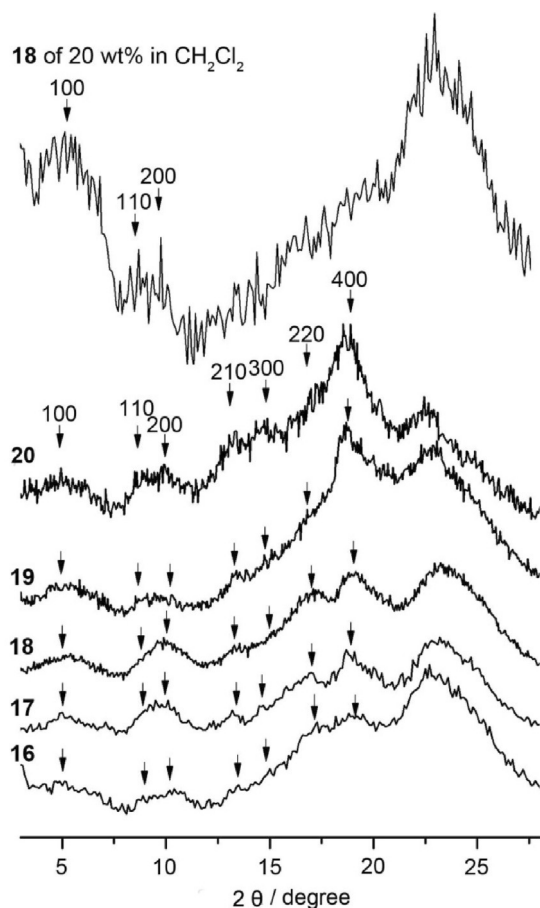


Figure 5. XRD patterns of the LC phase of 20 wt% **18** in CH_2Cl_2 and solids **16–20** prepared by slow evaporation of LC phases in CH_2Cl_2 at room temperature. The (100), (110), (200), (210), (300), (220) and (400) peaks correspond to a hexagonal accumulation structure.

same accumulation structure. Take solid **18** as an example, seven diffraction peaks at d spacings of 1.70, 1.00, 0.88, 0.66, 0.58, 0.51 and 0.46 nm with a ratio of $1:1/\sqrt{3}:1/2:1/\sqrt{7}:1/3:1/\sqrt{12}:1/4$ corresponded to a hexagonal columnar structure.^[20] The postulated accumulation model was similar to those previously described in the references.^[10,11] The helical hydrocarbon backbones stack atop one another along the same helix axis to form a long column, and seven long columns further assemble laterally. Notably, solvent molecules in LC samples need be removed before PXRD experiments. This possibly caused the accumulation structure to become partially destroyed, because solvent molecules could take part in the assembly. So, it was reasonable that the acquired signal peaks

became broadened. The (110) peak was relatively weak. Fortunately, the (220) peak, characteristic of hexagonal accumulation, was clear. The strong diffraction peak at 0.38 nm could possibly be attributed to the screw pitch or the π - π stacking. In situ measurement of the LC sample was also carried out (Figure 5). The noise hid many signal peaks, owing to the scattering of solvent molecules. However, we also could discriminate the (100), (110) and (200) peaks, because their relative positions are similar to those of solid samples. In particular, the diffraction peak at 0.38 nm that symbolises the screw pitch was very strong. Interestingly, the PXRD pattern of xerogel **15** exhibited three peaks at d spacings of 2.32, 1.15 and 0.77 nm, corresponding to a lamellar architecture with a reciprocal spacing ratio of 1:1/2:1/3 (Figure 6). This is a rare example of the sheet-like tertiary structure of an “abiotic” foldamer.^[6h]

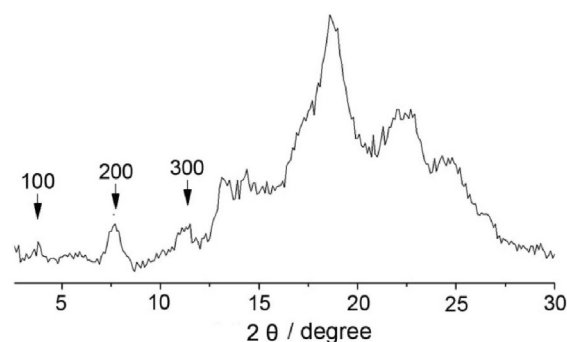


Figure 6. PXRD pattern of xerogel **15**. The (100), (200) and (300) peaks correspond to a lamellar structure.

When lyotropic LC phases were formed from helical peptides, the formation of rod-shaped assemblies was usually observed.^[7g] Herein, scanning electron microscopy (SEM) and transmission electron microscopy (TEM) were also used to explore evidence of LC formation. The SEM images of **16–20** in the LC phase explicitly displayed many thin nanofibres (Figure 7), indicating a typical LC microstructure. In contrast, tetramer **11** did not display any rod-shaped assembly. The TEM pictures exhibited similar species (Figure 8). The SEM and TEM pictures of gel **15** also displayed many entangled nanofibres (Figures 7a and 8a).

We also measured the ultraviolet (UV) absorption and circular dichroism (CD) spectra of these oligomers at different concentrations to further evaluate their assembly behaviours in solution. The UV spectra of **17** in CH_2Cl_2 showed a maximum absorption at 311 nm, ascribed to PE and *p*-aminobenzoic ester chromophores (Figure 9a). The CD spectra of 0.05 mM or 0.5 mM **17** in CH_2Cl_2 showed the positive Cotton effects in the range of 270–320 nm (Figure 9a). From 0 to 0.5 mM, the signal intensities were approximately linearly dependent on concentration. The UV and CD spectra of **15**, **16**, **18**, **19**, and **20** in dilute solutions were similar to those of **17** (Figures 9b and S4–S7). Notably, the molar absorption coefficients of **17** in some good solvents such as THF or DMSO were almost the same as that in CH_2Cl_2 , although the UV signals exhibited

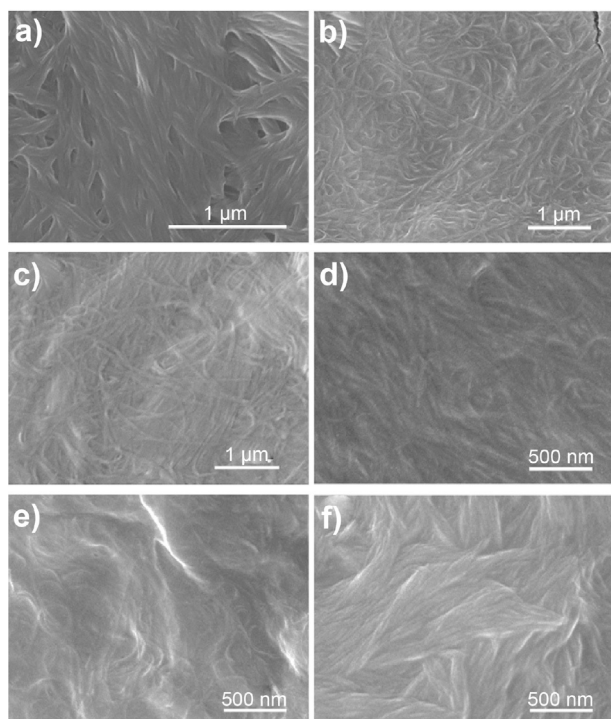


Figure 7. SEM images of a) xerogel 15, and solids b) 16, c) 17, d) 18, e) 19, and f) 20 prepared from slow evaporation of LC phases.

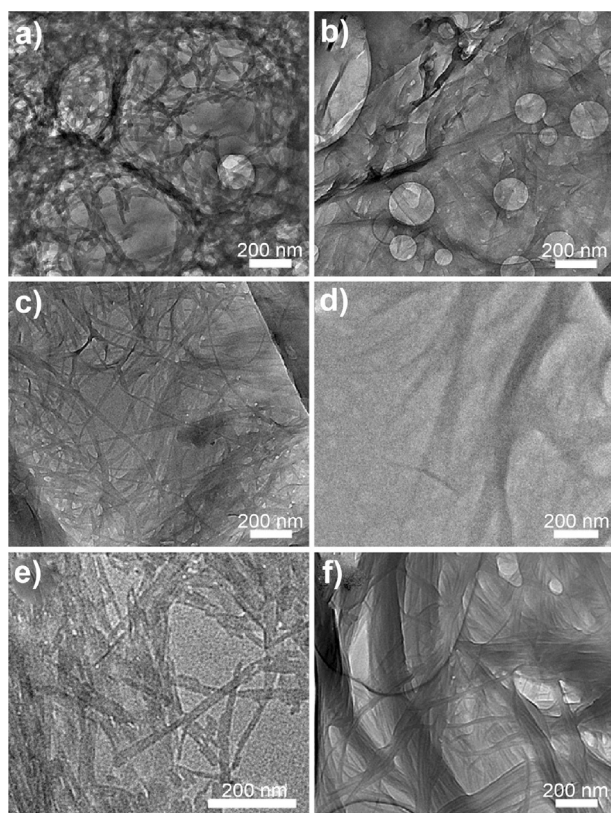


Figure 8. TEM pictures of a) gel 15, and LCs b) 16, c) 17, d) 18, e) 19 and f) 20.

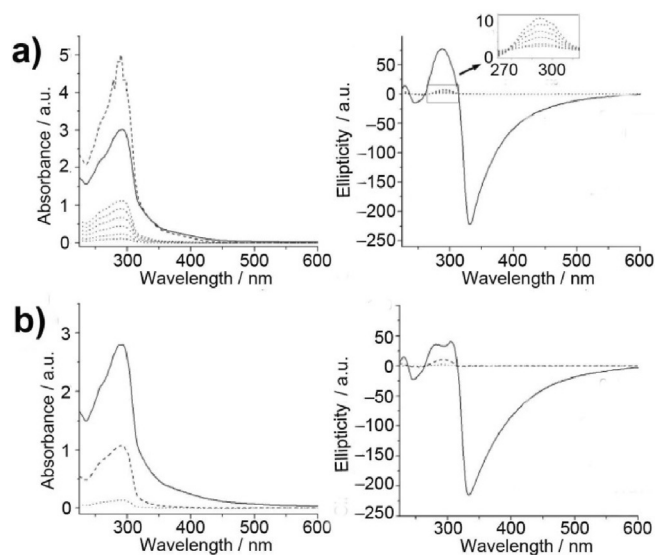


Figure 9. UV and CD spectra of a) 17 of 0.05–0.5 mm (dot), 4 mm (dash), 5 mm (solid); b) 19 of 0.05 mm (dot), 0.5 mm (dash), 5 mm (solid) in CH_2Cl_2 at room temperature. A 0.1 mm cuvette was used. The UV spectrum of 4 mm 17 at 270–320 nm displayed noise. The CD spectrum of 4 mm 17 is not shown, because it only displayed strong noise.

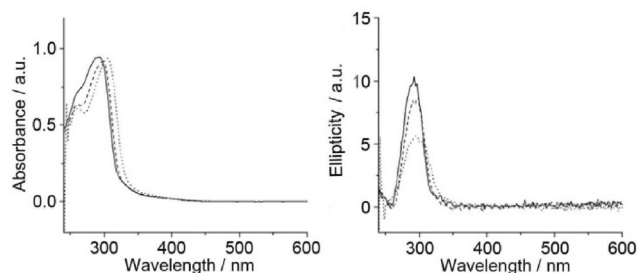


Figure 10. The UV and CD spectra of 0.05 mm 17 in CH_2Cl_2 (solid), THF (dash) and DMSO (dot) at room temperature. A 1 mm cuvette was used.

a slight shift and the amplitude of the CD signal also changed (Figure 10). These observations indicated that the foldamers were random coils in dilute solutions.

It is usually difficult to analyse UV and CD at high concentrations. However, we could obtain useful structural information. The hypochromic effect, observed as the reduction in optical absorption intensity, is a powerful indicator of the oriented chromophores.^[4a] Hypochromic effects are sensitive to the distance, r , between chromophores and their relative orientations. Figure 9a shows that the absorbance value (>4) at 311 nm was out of measuring range when the concentration of 17 was 4 mm. Interestingly, when the concentration of 17 reached the LC critical value of 5 mm (ca. 1 wt%), the absorbance abruptly decreased. This evident hypochromic effect can be explained by the formation of a compact helical backbone through intramolecular π - π stacking. The CD spectra of 5 mm 17 in CH_2Cl_2 displayed very strong negative Cotton effects at 330–450 nm and a positive effect at 260–320 nm. This was mainly attributed to the M_p -PE backbone predominantly in

one helical sense and consequent orderly arrangement of side chains. The change of CD signal to a larger amplitude is also attributed to the chiral cumulative effect or chiral amplification.^[21] The linear dichroism (LD) signals at the LC concentration are very weak (Figure S8), indicating that CD data are reliable. Similar phenomena were observed for compound **19** (Figure 9b). However, it was not possible to obtain the UV and CD spectra for **16**, **18** and **20** in the LC state, because the values of the critical concentration were high enough to surpass the measurement range.

Notably, when the LC phase of **17** was diluted 100 times, a strong bisignated CD signal was still observed and almost no change occurred for at least 2 weeks (Figures 11 a and S9). The SEM images of compound **17**, prepared from dilute solution, displayed many thin nanofibres (Figure 12 a). These observa-

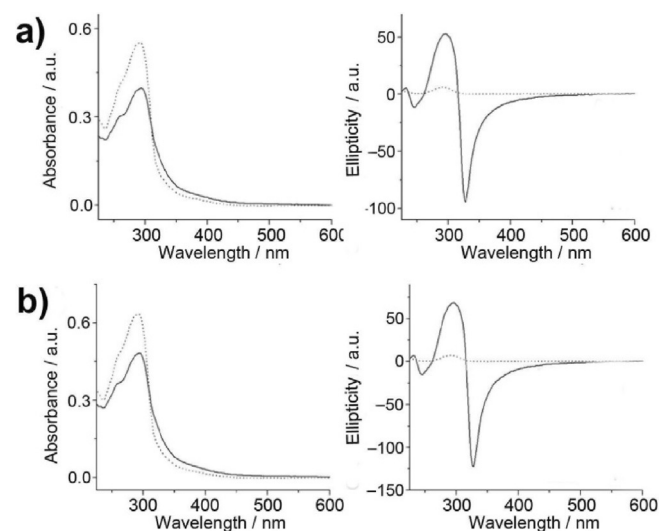


Figure 11. UV and CD spectra of diluted LC solution of a) **17** and b) **19** in CH_2Cl_2 at room temperature before (solid) and after (dot) the samples were heated for 2 min at 100°C . Concentration: 0.05 mM. A 1 mm cuvette was used.

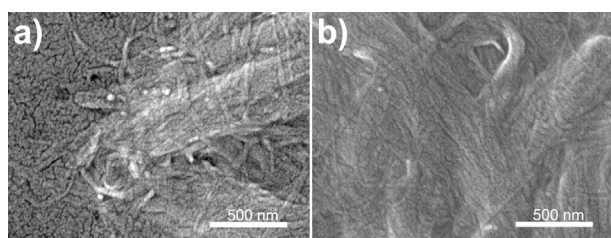


Figure 12. SEM images of assemblies of a) **17** and b) **19** on silicon chip prepared by fast casting a diluted LC solution in CH_2Cl_2 (0.05 mM).

tions suggested that the hexagonal structure of **17** was maintained. After the diluted sample was heated for 2 min at 100°C , the bisignated CD signal disappeared and the UV absorption was evidently strengthened (Figure 11 a), indicating that the foldamer in a random coil was recovered. Similar phenomena were also observed for compound **19** (Figures 11 b

and 12 b). Furthermore, the dynamic light scattering (DLS) experiments showed that the average hydrodynamic radius decreased after heating the dilute LC solution (Figure 13). This observation was in accordance with the abovementioned analysis. Notably, DLS experiments were not used to measure LC

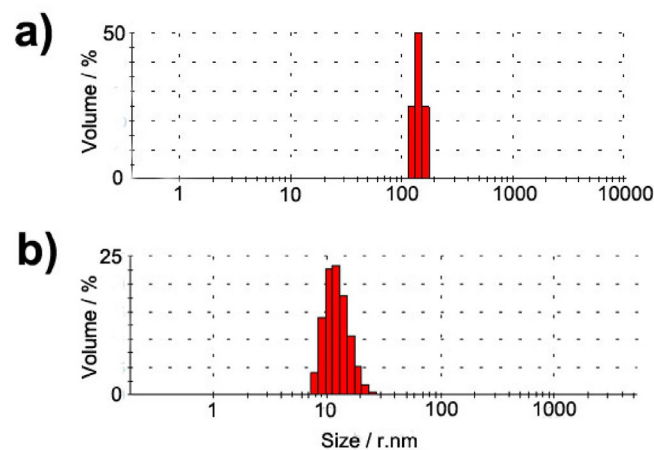


Figure 13. DLS diagrams of diluted LC solution of **17** in CH_2Cl_2 : a) before and b) after heating.

samples, because the concentrations were too high. In contrast, when the LC phases of oligomers **16**, **18**, and **20** were diluted, the CD spectra only presented patterns belonging to a random coil (Figure S10). This was possibly caused by the higher solubility of these oligomers with TIPS groups. In addition, the larger volume of TIPS groups on the terminal alkyne could affect the accumulation of these foldamer backbones and side chains.

Referring to the single-crystal structure of (*R*)-dimer **5** (Figure 1), there is an angle of approximately 110° between two adjacent PE segments in oligo(*Mp*-PE)s. In contrast, the value is 120° for oligo(*m*-PE)s. It is known that oligo(*m*-PE) has a helical turn of approximately six repeating units.^[11,22] We evaluated that a helix turn of more compact oligo(*Mp*-PE)s could contain five repeating units, referring to molecular shapes of a dimer in the crystal and an intramolecular π - π stacking distance (Figures 14 a and 14 b). When aggregated, the oligo(*Mp*-PE)s with six or eight repeating units can form a helical chain. In contrast, intramolecular π - π stacking is difficult for the pentamer.

According to XRD data, there is a distance of approximately 2.0 nm between two adjacent long columns in the hexagonal structure. It could reasonably be assumed that long columns have a diameter close to cyclic *Mp*-PE pentamer (ca. 1.5 nm, Figure 15). Moreover, the side chain has a length of 0.8–0.9 nm, according to crystal structure of (*R*)-dimer **5**. So, the superposition of side chains between adjacent long columns should exist (Figures 14 c and 14 d). This would improve contact in the aggregate, favouring the stabilisation of the whole hexagonal system. In contrast, there is almost no superposition between adjacent long columns in a hexagonal model of poly(*m*-PE).^[11] Notably, the thinnest fibre, with a diameter of

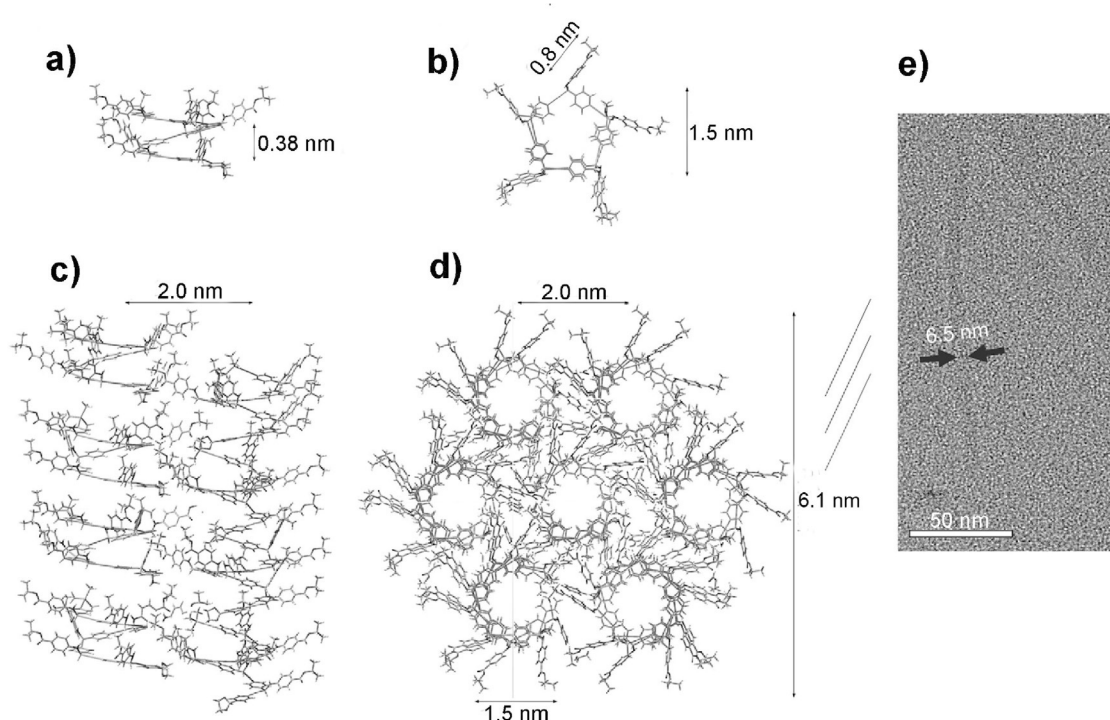


Figure 14. Schematic representation of a single-molecular helical model [side view (a); top view (b)], two adjacent long columns (c) and the hexagonal accumulation model (d) of octamer **17**. TEM image with the thinnest fibre (e) of octamer **17**. Helical pitch: approximately 0.38 nm; side chain length: 0.8 nm; diameter of central channel: 1.5 nm; distance between two adjacent long columns: 2.0 nm. These data were obtained according to XRD analysis, the crystal structure of dimer **5** and theoretical calculations.

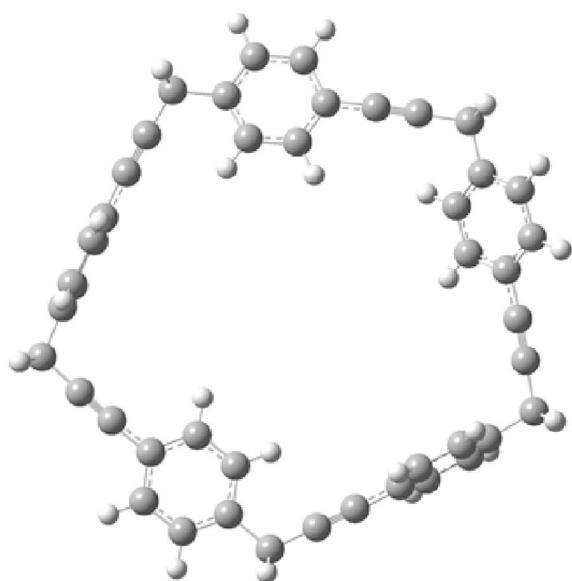


Figure 15. The energy minimisation geometrical model of the cyclic *Mp*-PE pentamer. Geometry optimisation and the harmonic vibrational frequency model were performed at the B3LYP/3-21G level using the Gaussian 09 program package. The length of the *Mp*-PE segment is approximately 0.88 nm, and the diameter of this pentamer is around 1.5 nm.

approximately 6.5 nm in the TEM images, almost matched the size of the smallest hexagonal aggregate unit (Figure 14e).

3. Conclusions

We have successfully synthesised a series of simple chiral *Mp*-PE oligomers with 4-isopropoxycarbonyl phenylamino side groups. The construction of this novel *Mp*-PE structure by using the asymmetric Mannich addition approach is unprecedented. Hexamer and octamers can form the hexagonal lyotropic LC phase in CH_2Cl_2 , whereas the pentamer forms a lamellar gel. According to the experimental results and theoretical calculations, we clearly obtain a folding and further aggregating model. Owing to the more compact backbone and more rigid side chain, the hexagonal aggregate is quite stable in CH_2Cl_2 , although only weak van der Waals interactions exist between long columns. This makes the formation of rod-shaped assemblies possible. These results could provide a new design avenue to useful tertiary assemblies from classic “abiotic” foldamers. In our laboratory, the exploration for other types of *Mp*-PE oligomers is underway.

Experimental Section

All reagents were obtained from commercial suppliers and, with the exception of CH_2Cl_2 , were used without further purification. CH_2Cl_2 was purified by distillation according to standard methods. All air-sensitive reactions were carried out under a N_2 atmosphere. Column chromatography was performed on 100–200 mesh silica gel. The ^1H NMR spectra were recorded at 400 MHz (Bruker AV) and the ^{13}C NMR spectra were recorded at 100 MHz with TMS as the internal standard. All shifts are given in ppm. All coupling con-

stants (J values) are reported in Hertz (Hz). Fourier-transform infrared spectra were recorded on a Bruker Vertex70 Win-IR instrument. High-resolution mass spectra were obtained by using IonSpec7.0T MALDI-FTICRMs. Optical rotation was measured by the PerkinElmer 341 LC polarimeter, using the 10 or 1 cm optical rotation pool. SEM was performed on an XL 30 scanning electron microscope (Micrion FEI PHILIPS). A drop of the LC phase or a little gel was put on the glass sheet and dried in air at room temperature for 5 h. The sample was then coated with Pt/Pd in the ion coater for 40 s. TEM images were obtained by using a JEM-1011 electron microscope operating at an acceleration voltage of 100 kV. A carbon-coated copper grid was quickly put into the LC phase or gel for less than 1 s and dried in air at room temperature for 5 h. CD and LD spectra were obtained by using a Biologic Science MOS-450 scanning spectrometer. LD is the difference between absorption of light polarised parallel and polarised perpendicular to an orientation axis. PXRD measurements were carried out on a Bruker D8 ADVANCE diffractometer, using Cu K α radiation ($\lambda = 0.154$ nm). X-ray crystallographic analysis was performed on a Bruker SMART APEX II CCD diffractometer with graphite-monochromated Mo K α radiation ($\lambda = 0.71073$ Å) operated at 2.0 kW (50 kV, 40 mA). The structures were solved by using direct methods with the program SHELXL-97 and refined anisotropically through full matrix least squares with F^2 values and SHELXL-97. Hydrogen atoms were located at the expected geometry and were only isotropically refined.

General Experimental Procedures for the Asymmetric Mannich Reaction

Aldehyde, alkyne, amine, CuBF₄(CH₃CN)₄, tri(*o*-tolyl)phosphine, *N*-Boc-L-proline and 3 Å molecular sieves (MS) powder were added into a dried round-bottomed flask. After the atmosphere was replaced with nitrogen twice, dry CH₂Cl₂ was introduced. Then, the mixture was stirred for 7 days. After the removal of the MS, the resulting green solution was diluted with CH₂Cl₂, washed with saturated aqueous NaHCO₃, dried over Na₂SO₄, filtered, and concentrated under reduced pressure. The residue was purified by using silica gel column chromatography to afford the oligomers. See the Supporting Information for further experimental details.

General Experimental Procedures for Deprotection of Protected Aldehyde and Alkyne Compounds

Acetal, CsF, AcOH and THF were added to a reaction tube. The mixture was stirred for 5 h at 60 °C in the sealed tube. The solvent was removed under reduced pressure, and then CH₂Cl₂ was added. The resulting suspension was washed with saturated aqueous NaHCO₃, dried over Na₂SO₄, filtered, and concentrated under reduced pressure. The residue was purified by using silica gel column chromatography to afford the aldehyde product. See the Supporting Information for further experimental details.

The silane-protected alkyne compound, THF, H₂O and BF₃-Et₂O were added to a reaction tube. The mixture was stirred for 5 h at 60 °C in the sealed tube. The reaction solution was concentrated under reduced pressure and dissolved again in CH₂Cl₂. The resulting solution was washed with saturated aqueous NaHCO₃, dried over Na₂SO₄, filtered, and concentrated under reduced pressure. The residue was purified by using silica gel column chromatography to afford the alkyne product. See the Supporting Information for further experimental details.

Acknowledgements

The authors thank the National Natural Science Foundation of China (21374113) for financial support. The authors thank the help of Dr. Zongjun Li and Professor Xiang Gao for computing the energy minimisation geometrical model of the cyclic Mp-PE pentamer.

Keywords: aggregation · asymmetric synthesis · helices · liquid crystals · supramolecular chemistry

- [1] a) S. H. Gellman, *Acc. Chem. Res.* **2007**, *46*, 173; b) R. P. Cheng, S. H. Gellman, W. F. DeGrado, *Chem. Rev.* **2001**, *101*, 3219.
- [2] D. J. Hill, M. J. Mio, R. B. Prince, T. S. Hughes, J. S. Moore, *Chem. Rev.* **2001**, *101*, 3893.
- [3] E. Yashima, K. Maeda, H. Lida, Y. Furusho, K. Nagai, *Chem. Rev.* **2009**, *109*, 6102.
- [4] a) J. C. Nelson, J. G. Saven, J. S. Moore, P. G. Wolynes, *Science* **1997**, *277*, 1793; b) C. R. Ray, J. S. Moore, *Adv. Polym. Sci.* **2005**, *177*, 91; c) M. T. Stone, J. M. Heemstra, J. S. Moore, *Acc. Chem. Res.* **2006**, *39*, 11.
- [5] a) V. Berl, I. Huc, R. G. Khoury, M. J. Krische, J. M. Lehn, *Nature* **2000**, *407*, 720; b) I. Huc, *Eur. J. Org. Chem.* **2004**, 17.
- [6] a) E. Yashima, K. Maeda, Y. Okamoto, *Nature* **1999**, *399*, 449; b) K. Shimomura, T. Ikai, S. Kanoh, E. Yashima, K. Maeda, *Nat. Chem.* **2014**, *6*, 429; c) R. B. Prince, S. A. Barnes, J. S. Moore, *J. Am. Chem. Soc.* **2000**, *122*, 2758; d) L. Byrne, J. Sol, T. Boddaret, T. Marcelli, R. W. Adams, G. A. Morris, J. Clayden, *Angew. Chem. Int. Ed.* **2014**, *53*, 151; *Angew. Chem.* **2014**, *126*, 155; e) S. Kwon, H. S. Shin, J. Gong, J. H. Eom, A. Jeon, S. H. Yoo, I. S. Chung, S. J. Cho, H. S. Lee, *J. Am. Chem. Soc.* **2011**, *133*, 17618; f) J. Buratto, C. Colombo, M. Stupfel, S. J. Dawson, C. Dolain, B. L. Estaintot, L. Fischer, T. Granier, M. Laguerre, B. Gallois, I. Huc, *Angew. Chem. Int. Ed.* **2014**, *53*, 883; *Angew. Chem.* **2014**, *126*, 902; g) J. D. Sadowsky, M. A. Schmitt, H. S. Lee, N. Umezawa, S. Wang, Y. Tomita, S. H. Gellman, *J. Am. Chem. Soc.* **2005**, *127*, 11966; h) G. Guichard, I. Huc, *Chem. Commun.* **2011**, 47, 5933; i) N. Chandramouli, Y. Ferrand, G. Lautrette, B. Kauffmann, C. D. Mackereth, M. Laguerre, D. Dubreuil, I. Huc, *Nat. Chem.* **2015**, *7*, 334.
- [7] a) C. Robinson, *Trans. Faraday Soc.* **1956**, *52*, 571; b) C. Robinson, *Tetrahedron* **1961**, *13*, 219; c) E. G. Bellomo, P. Davidson, M. Impéror-Clerc, T. J. Deming, *J. Am. Chem. Soc.* **2004**, *126*, 9101–9105; d) S. M. Yu, V. P. Conticello, G. Zhang, C. Kayser, M. J. Fournier, T. L. Mason, D. A. Tirrell, *Nature* **1997**, *389*, 167; e) W. C. Pomerantz, N. L. Abbott, S. H. Gellman, *J. Am. Chem. Soc.* **2006**, *128*, 8730; f) W. C. Pomerantz, V. M. Yuwono, C. L. Pizze, J. D. Hartgerink, N. L. Abbott, S. H. Gellman, *Angew. Chem. Int. Ed.* **2008**, *47*, 1241; *Angew. Chem.* **2008**, *120*, 1261; g) W. C. Pomerantz, V. M. Yuwono, R. Drake, J. D. Hartgerink, N. L. Abbott, S. H. Gellman, *J. Am. Chem. Soc.* **2011**, *133*, 13604.
- [8] a) D. Haldar, C. Schmuck, *Chem. Soc. Rev.* **2009**, *38*, 363; b) Y. Tanaka, H. Katagiri, Y. Furusho, E. Yashima, *Angew. Chem. Int. Ed.* **2005**, *44*, 3867; *Angew. Chem.* **2005**, *117*, 3935; c) Y. Ferrand, A. M. Kendhale, J. Garric, B. Kauffmann, I. Huc, *Angew. Chem. Int. Ed.* **2010**, *49*, 1778; *Angew. Chem.* **2010**, *122*, 1822; d) Q. Gan, C. Bao, B. Kauffmann, A. Grélard, J. Xiang, S. Liu, I. Huc, H. Jiang, *Angew. Chem. Int. Ed.* **2008**, *47*, 1715; *Angew. Chem.* **2008**, *120*, 1739; e) W. Cai, G. T. Wang, Y. X. Xu, X. K. Jiang, Z. T. Li, *J. Am. Chem. Soc.* **2008**, *130*, 6936; f) L. A. Cuccia, E. Ruiz, J. M. Lehn, J. C. Homo, M. Schmutz, *Chem. Eur. J.* **2002**, *8*, 3448.
- [9] N. Saito, K. Kanie, M. Matsuura, A. Muramatsu, M. Yamaguchi, *J. Am. Chem. Soc.* **2015**, *137*, 6594.
- [10] M. J. Mio, R. B. Prince, J. S. Moore, C. Kübel, D. C. Martin, *J. Am. Chem. Soc.* **2000**, *122*, 6134.
- [11] M. Banno, T. Yamaguchi, K. Nagai, C. Kaiser, S. Hecht, E. Yashima, *J. Am. Chem. Soc.* **2012**, *134*, 8718.
- [12] L. Onsager, *Ann. N. Y. Acad. Sci.* **1949**, *51*, 627–659.
- [13] a) R. B. Prince, L. Brunsveld, E. W. Meijer, J. S. Moore, *Angew. Chem. Int. Ed.* **2000**, *39*, 228; *Angew. Chem.* **2000**, *112*, 234; b) L. Brunsveld, E. W. Meijer, R. B. Prince, J. S. Moore, *J. Am. Chem. Soc.* **2001**, *123*, 7978; c) M. S. Gin, T. Yokozawa, R. B. Prince, J. S. Moore, *J. Am. Chem. Soc.*

- 1999, 121, 2643; d) D. J. Hill, J. S. Moore, *Proc. Natl. Acad. Sci. USA* **2002**, 99, 5053; e) M. S. Gin, J. S. Moore, *Org. Lett.* **2000**, 2, 135–138.
- [14] A. Aggeli, I. A. Nyrkova, M. Bell, R. Harding, L. Carrick, T. C. B. McLeish, A. N. Semenov, N. Boden, *Proc. Natl. Acad. Sci. USA* **2001**, 98, 11857.
- [15] Y. Lu, T. C. Johnstone, B. A. Arndtsen, *J. Am. Chem. Soc.* **2009**, 131, 11284.
- [16] All endeavours to separate (*R,R,R,R,R*)/(*R,R,R,S,R*)-hexamer, (*R,R,R,R,R,R,R*)/(*R,R,R,S,R,R,R*)-octamers by HPLC failed. This possibly was because of the very small difference between the diastereomers.
- [17] N. H. Hartshorne, A. Stuart, *Crystals and the Polarizing Microscope*, American Elsevier, New York, **1970**.
- [18] I. Dierking, *Textures of Liquid Crystals*, Wiley-VCH, Weinheim, **2003**.
- [19] a) J. C. Blackburn, P. K. Kilpatrick, *Langmuir* **1992**, 8, 1679; b) N. Boden, S. A. Corne, K. W. Jolley, *J. Phys. Chem.* **1987**, 91, 4092.
- [20] P. Alexandridis, U. Olsson, B. Lindman, *Langmuir* **1998**, 14, 2627.
- [21] N. Berova, K. Nakanishi, R. W. Woody, *Circular Dichroism: Principles and Applications*, Wiley-VCH, New York, **2000**.
- [22] K. Matsuda, M. T. Stone, J. S. Moore, *J. Am. Chem. Soc.* **2002**, 124, 11836.
- [23] CCDC 1408695 contains the supplementary crystallographic data for this paper. These data can be obtained free of charge from The Cambridge Crystallographic Data Centre.

 Received: January 20, 2016

Published online on April 27, 2016